Assessing the impact of granular anaerobic membrane bioreactor intensification on treatment performance, membrane fouling and economic balance

Lucie Sanchez, Sergi Vinardell, Jules Charreton, Marc Heran, Geoffroy Lesage

▶ **To cite this version:**

HAL Id: hal-04051972

https://hal.umontpellier.fr/hal-04051972v1

Submitted on 11 Apr 2023

Assessing the impact of granular anaerobic membrane bioreactor intensification on treatment performance, membrane fouling and economic balance

Lucie Sanchez[a], Sergi Vinardell[b,c], Jules Charreton[a], Marc Heran[a], Geoffroy Lesage[a,*]

[a] Institut Européen des Membranes (IEM), Université de Montpellier, CNRS, ENSCM, Montpellier, France

[b] Chemical Engineering Department, Escola d'Enginyeria de Barcelona Est (EEBE), Universitat Politècnica de Catalunya (UPC)-BarcelonaTECH, C/ Eduard Maristany 10-14, Campus Diagonal-Besòs, Barcelona, Spain.

[c] Barcelona Research Center for Multiscale Science and Engineering, Campus Diagonal-Besòs, Barcelona, Spain.

*Corresponding author (e-mail: geoffroy.lesage@umontpellier.fr)

ABSTRACT

Anaerobic membrane bioreactors (AnMBRs) have attracted much attention for mainstream domestic wastewater treatment. However, membrane fouling, operating costs, energy consumption and low filtration flux are important challenges slowing the scale-up of the technology. In this study and for the first time, granular sludge, submerged membrane, no gas sparging and low permeate flux were chosen to mitigate membrane fouling and to improve the energy and economic balance of an AnMBR. A granule-based AnMBR (G-AnMBR) was operated under four organic loading rates (between 0.5 and 1.6 kgCOD.m^{-3}.d^{-1}) with hydraulic retention times ranged from 13.9 to 4.9 hours, and instantaneous permeate flux levels ($Jp_{20,inst}$) ranged from 2.8 to 6.0 LMH to evaluate OLR impact on anaerobic digestion performance, membrane fouling extent and economic balance. Results show that COD removal rates above

24 83% were achieved during the four experimental periods. Membrane fouling was directly

25 correlated to the flux and OLR and increased from 0.03 to 2.86 kPa.d^{-1} as the $Jp_{20,inst}$ increased

26 from 2.8 to 6.0 LMH and the OLR increased from 0.5 to 1.6 kgCOD.m^{-3}.d^{-1}, respectively. In

27 all the periods, macromolecules and colloidal proteins were the major foulants deposited on the

28 membrane. Most of the fouling was reversible and was easily removed by physical cleaning

29 (>97.7%). A preliminary economic assessment revealed that the permeate flux and OLR are

30 key economic drivers for the G-AnMBR economic balance and allowed to define the

31 satisfactory compromise between membrane purchase and chemical consumption for the long-

32 term control of membrane fouling.

33 **KEYWORDS**

34 filtration flux; membrane fouling; techno-economic evaluation; granular sludge; anaerobic

35 digestion

36 ## 1. Introduction

37 Anaerobic membrane bioreactors (AnMBRs) have gained interest over conventional aerobic

38 biotechnologies by combining the advantages of anaerobic processes with membrane

39 technology. Anaerobic digestion reduces energy demand, produces fewer bio-solids, reduces

40 sludge disposal costs and generates bioenergy through the complete conversion of organic

41 materials into methane (Vinardell et al., 2020). Micro- or ultrafiltration membranes offer strong

42 retention of particles and microorganisms, leading to higher biomass concentration and longer

43 sludge retention time (SRT), which is beneficial for slow-growth anaerobic microorganisms

44 and the quality of the permeate. Therefore, the AnMBR is a cost-effective alternative that allows

45 conversion of wastewater organic material into renewable methane energy while achieving a

46 high-quality effluent, free of suspended solids and pathogens, which could be easily reused for

47 various applications (Aslam et al., 2022; Vinardell et al., 2020).

2

48 Nonetheless, the AnMBR still faces some issues that have hindered its large-scale development

49 for domestic wastewater treatment. The main operational and technical challenges in its

50 application to domestic wastewater have been linked to low psychrophilic temperatures, low-

51 strength wastewater, dissolved methane and membrane fouling, among others (Aslam et al.,

52 2022; Lei et al., 2018; Vinardell et al., 2020). The large amount of dilute domestic wastewater

53 results in lower methane conversion rates ($L\text{-}CH_4.m^{-3}$) and higher quantities of methane lost

54 within the effluent (Maaz et al., 2019). The loss of methane in the liquid phase diminishes the

55 potential for energy recovery and produces direct greenhouse gas emissions (Smith et al., 2012).

56 Membrane fouling has a high impact on the capital and operational costs of AnMBR due to its

57 effect on permeate flux, membrane lifespan and energy demand (Maaz et al., 2019; Smith et

58 al., 2012). Accordingly, all these factors decrease energy recovery efficiency and increase

59 energy demand (e.g., membrane fouling mitigation, dissolved methane recovery, etc.), which

60 reduce the economic and energy advantages of AnMBRs.

61 In recent years, several studies have applied lab- and pilot-scale AnMBRs to low-strength

62 wastewater treatment at psychrophilic temperatures. As described in Table 1, various

63 configurations and fouling control strategies have been tested to achieve high efficiencies of

64 organic matter removal and methane conversion while mitigating membrane fouling. The

65 chemical oxygen demand (COD) removal efficiencies obtained through AnMBR processes

66 have typically ranged between 85% and 95% at both lab- and pilot-scales under sub-optimal

67 conditions (i.e., ambient temperature and low-strength wastewater) (Table 1), suggesting that

68 efficient methane yield and conversion rates can be reached (Chen et al., 2017b; Nie et al.,

69 2017; Shin et al., 2021). Then, many investigations have focused on AnMBR configuration and

70 membrane fouling (Table 1). The different system configurations have mainly differed in terms

71 of (i) integration of the membrane (i.e., submerged, external submerged, side-stream), (ii) type

72 of anaerobic bioreactor (i.e., continuous stirred tank reactor [CSTR], upflow anaerobic sludge

73   blanket [UASB], etc.), (iii) membrane module type (i.e., flat sheet, hollow fiber, etc.), (iv)

74   fouling control strategies and (v) operating conditions. Innovative strategies have been

75   implemented to better control membrane fouling (Aslam et al., 2017), including rotating

76   membrane (Ruigómez et al., 2016a, 2016b), dynamic membrane (Hu et al., 2018; Quek et al.,

77   2017; Yang et al., 2020), granular activated carbon media (Evans et al., 2019), sponge media

78   (Chen et al., 2017b) and granular biomass (Chen et al., 2017a; Gouveia et al., 2015). However,

79   gas sparging remains the most frequently used approach for long-term mitigation of membrane

80   fouling despite its energy consumption, which amounts to up to 70% of the total AnMBR

81   energy input (Batstone and Virdis, 2014; Smith et al., 2014).

82   Among the innovative strategies that have been tested, the use of granular biomass is an

83   attractive cost-effective solution, as it reduces energy consumption for the control of membrane

84   fouling (Martin-Garcia et al., 2013) and does not involve additional material costs or technical

85   complexity. Granulation is a process resulting in dense granule-shaped biomass which

86   improves biological activity and strength (van Lier et al., 2008). Unlike the suspended sludge

87   configuration, a granule-based AnMBR (G-AnMBR) helps to lower the concentration of

88   suspended solids in contact with the membrane, improving the control of membrane fouling

89   and decreasing cake-layer formation (Vinardell et al., 2022). However, the G-AnMBR

90   configuration does not fully overcome membrane fouling, as complete membrane retention

91   leads to the accumulation of colloidal and fine particulate matter, either introduced from the

92   influent or released from the granular sludge bed due to too strong hydrodynamic conditions

93   (Anjum et al., 2021; Vinardell et al., 2022). To mitigate membrane fouling, gas sparging is also

94   used in this granule-based configuration. Kong et al. (2021b) reached the maximal TMP (235

95   mbar) in 8 days at a filtration flux of 17.8 $L.m^{-2}.h^{-1}$ (LMH) and at a specific gas demand (SGD)

96   of 0.75 $m^3.m^{-2}.h^{-1}$. Wang et al. (2018) applied a SGD of 0.2 $m^3.m^{-2}.h^{-1}$ and achieved the

97   maximal TMP (550 mbar) in less than one day when the flux was increased from 5 to 10 LMH.

98 Gas sparging is cost-intensive and damages granule structures which increases granules fines

99 and dissolved and colloidal organic matter (DCOM) release in the bulk (Martin-Garcia et al.,

100 2013). For these reasons, avoiding the use of gas sparging may assist in maintaining the

101 integrity and the particle size distribution of granules, with a substantial benefit in energy

102 consumption (Sanchez et al., 2022). In addition, it appears that a high permeate flux cannot be

103 maintained, which reduces the competitiveness of G-AnMBR compared to conventional

104 processes (AeMBR). Hence, it is necessary to explore the behavior of the process following the

105 increase of permeate flux and, more specifically, to characterize membrane fouling and its

106 economic and energetic implications during process intensification.

107 This study aimed to evaluate the impact of G-AnMBR process intensification – by increasing

108 the organic loading rate and the permeate flux – on anaerobic digestion performance, membrane

109 fouling and process economics. The G-AnMBR system was operated without gas sparging to

110 limit the energy consumption during domestic wastewater treatment and ambient temperature.

111 To the best of our knowledge, the impact of process intensification on membrane fouling of a

112 G-AnMBR in submerged mode and operated without gas sparging, has not yet been evaluated.

113 For this reason, a G-AnMBR without gas sparging for fouling control was operated under four

114 permeate flux conditions of 2.8, 3.6, 4.1 and 6.0 LMH and OLR of 0.5, 0.8, 1.0, 1.6 kgCOD.m^{-3}.d^{-1}.

115 Anaerobic digestion performance and membrane fouling behavior were assessed. Based

116 on the experimental results, an economic evaluation was conducted to elucidate how the

117 intensification of the process (through OLR and permeate flux increase) might influence the

118 operational and capital costs of a G-AnMBR operated under low filtration rates.

119

Table 1 – Reactor configurations, operational parameters, treatment performance and membrane fouling strategies presented in recent AnMBR studies for domestic wastewater treatment at ambient temperature.

Reactor	Membrane setup	Fouling control strategy	Scale	Type of WW	COD_{in}	T	HRT	OLR	$COD_{removal}$	Methane yield	Flux	dTMP/dt	Reference
–	–	–	(liters)	–	$(mg.L^{-1})$	(°C)	(h)	$(kg.m^{-3}d^{-1})$	(%)	$(L\text{-}CH_4/gCOD_{removed})$	(LMH)	$(kPa.d^{-1})$	
UAGB	HF Sub.	Sponge cubes + intermittent cycle	(L) 3	Synthetic	330–370	20	12	–	93.7	0.156 (G)	5.3	0.5	(C. Chen et al., 2017b)
UAGB	HF Sub.	Granular sludge + Intermittent cycle	(L) 4	Synthetic	320–360	20	12	0.64–0.72 *	91.3	0.16 (G)	7	0.9	(C. Chen et al., 2017a)
UAGB	FS Sub.	Granular sludge + Intermittent cycle	(L) 6.2	Synthetic	300–350	25	13.9–4.9	0.5–1.6	83–93	70–77% [a] (G + D)	2.8–6	0.03–2.9	This study
UASB	FS sub.	Dynamic membrane	(L) 6.9	Raw	107–137	25–30	3–6	1.5–3.0	64–71	0.354 (–)	100	1.5–6.2	(Quek et al., 2017)
UAGB	HF Ext. sub.	Granular sludge + Intermittent cycle + gas sparging	(P) 72.5	Raw	221	16.3	8	<1.0 *	83	–	5–15	0.2–960 *	(Wang et al., 2018)
UAGB	HF Sub.	Granular sludge + Intermittent cycle + gas sparging	(P) 459	Raw	978	18	9.8–20.3	0.72–3.18	≈90	0.216–0.226 (G + D)	10–14	0.1–1.9	(Gouveia et al., 2015)
CSTR	FS Sub.	Intermittent cycle + gas sparging	(L) 6	Synthetic	700	25	8–48	0.35–2.1	≈95	0.277–0.328 (G + D)	1.1–6.5	–	(R. Chen et al., 2017a)
CSTR	FS Sub.	Intermittent cycle + gas sparging	(L) 6	Synthetic	700	25	8–48	0.35–2.1	>90	0.305–0.338 (G + D)	1.1–6.5	0.05–1.1 *	(R. Chen et al., 2017b)
CSTR	– Sub.	Gas sparging	(L) 6	Synthetic	492	25	24–12	3–6	97–94	89–84.7% [a] (G + D)	–	0.08–0.3	(Nie et al., 2017)
CSTR	FS Sub.	Intermittent cycle + gas sparging	(L) 40	Raw	428–477	14–26	12–48	0.23–0.9	69–89	0.28–0.35 [*,b] (G + D)	1.6–6.6	<0.06 *	(Plevri et al., 2021)
CSTR	HF Ext. sub.	Gas sparging	(P) 630	Synthetic	304–388	23	8.5	0.85–1.1 *	88–92	0.076–0.115 (G + D)	17	0.02–0.61	(Dong et al., 2016a, 2016b)

AFBR	HF Sub.	Granular activated carbon + gas sparging	(P) 990	Raw	210	13–32	3.9	1.3–1.4	86–90	0.17 (G)	7.6–7.9	–	(Evans et al., 2019)
AFBR	HF Ext. sub.	Intermittent cycle + gas sparging	(P) 4500	Raw	720–893	18–25	5.3–10	1.3–2.4	87–90	43–62 % [a] (G + D)	6.5–12.3	–	(Shin et al., 2021)
–	HF Sub.	Intermittent cycle + gas sparging	(P) 20	Raw	422	25	4–12	1.52–0.72	84–89	0.14–0.21 (G + D)	7.2–14.2	0.8–2.1	(Ji et al., 2021a)
–	HF Sub.	Gas sparging	(P) 20	Raw	422	15–25	6	0.15–0.18	77–90	0.06–0.17 (G + D)	9.5	0.1–13.0	(Ji et al., 2021b)
–	HF Sub.	Gas sparging	(P) 20	Raw	300–600	15	6–24	0.4–1.6	77–91	0.06–0.23 (G + D)	2.4–9.4	1.4–9.1	(Ji et al., 2022)
–	HF Sub.	Intermittent cycle + gas sparging	(P) 5000	Raw	403–461	25–27	6–24	0.37–1.84	90–93	0.16–0.26 (G + D)	4.4–17.8	0.08*–2.9	(Kong et al., 2021a) (Kong et al., 2021b)
–	HF Ext. sub.	Intermittent cycle + Gas sparging	(P) 40000	Raw	1235	27–30	24–60	–	92	0.21 (G + D)	15–23.5	0.04–0.22	(Robles et al., 2020)
–	HF Sub.	Intermittent cycle + Gas sparging	(P) 5000	Raw	414	25	8	1.2	90	0.222 (G + D)	10.85	0.04–0.2	(Rong et al., 2021)
–	HF Sub.	Rotating membrane	(L) 3	Raw	1462	19	33	–	91	0.154 * (G)	10	3.8*–14	(Ruigómez et al., 2016a, 2016b)
–	– Sub.	Gas sparging	(L) 6	Synthetic	491	10–25	6–48	0.25–1.0	71–98	32–77 % [a] (G)	–	0.17–0.72	(Watanabe et al., 2017)
UASB	– Sub.	Dynamic membrane	(L) 3.6	Raw	251–284	20–25	1–8	0.8–6.8	60–77	0.05–0.12 (G + D)	22.5–180	0.4–2.1	(Yang et al., 2020)

WW: wastewater; HRT: hydraulic retention time; OLR: organic loading rate; UAGB: upflow anaerobic granular bioreactor; UASB: upflow anaerobic sludge blanket; CSTR: completely stirred reactor; AFBR: anaerobic fluidized bed reactor ; FS: flat sheet; HF: hollow fiber; Sub.: membrane submerged in the bioreactor; Ext. sub.: membrane submerged in an external tank; L: lab-scale; P: pilot-scale; G: gaseous methane; D: dissolved methane.

* Values were calculated or approximated through data available in the publication.

[a] Methane conversion rate (%)

[b] Values were calculated based on the gas yield provided, considering a concentration of CH_4 of 70%.

2. Materials and methods

2.1 G-AnMBR setup

The G-AnMBR system consisted of a parallelepipedic tank (266 × 68 × 523 mm) with a working volume of 6.2 L that was operated in continuous mode for 357 days. The membrane module was immersed in the middle of the liquor (at a height of 205 mm from the bottom). The ultrafiltration membrane was a polyethersulfone (PES) flat-sheet membrane with a pore size of 0.04 µm (Microdyn Nadir®, Germany). The module was composed of six membrane sides, providing a total surface area of 0.34 m². The permeate was suctioned through a peristaltic pump (LeadFluid®, China) following an operation cycle of 8 min 15 s of filtration, 30 s of relaxation, 45 s of backwash and 30 s of relaxation. No method for the mitigation of membrane fouling was used apart from the intermittent cycle. The operation of the reactor was automatically managed by automation software developed by AC2I Automation (France). The reactor was thermoregulated at 25°C. The influent was fed at the bottom of the reactor by a peristaltic pump and diffused over the entire length by a pierced hollow tube (ø 1 mm) to minimize dead zones. Continuous recirculation from the top to the bottom of the reactor was used to provide an upflow liquid velocity (ULV) of 2.6 m/h (Boulenger and Gallouin, 2009) and no other mixing that this recirculation was operated. A schematic representation of the lab-scale reactor is shown in Fig. A1.

A complex synthetic influent was used to mimic domestic wastewater treatment, as described in previous studies (Layer et al., 2019; Sanchez et al., 2022). The feed solution was prepared every week with and stored at 4°C for one week. During the overall experiment, the average composition of the influent was approximately 290–350 mgCOD.L^{-1} for total COD (tCOD), 250–290 mgCOD.L^{-1} for soluble COD (sCOD), 40–60 mgCOD.L^{-1} for particulate COD (pCOD) and 160–210 mgCOD.L^{-1} for volatile fatty acids (VFA).

150   The G-AnMBR was inoculated with granular sludge from a mesophilic (35–38°C) UASB that

151   treats wastewater from a recycled paper factory (Saica Paper Champblain-Laveyron, France) at

152   a high organic loading rate (18 kgCOD.m^{-3}.d^{-1}). The granular sludge was acclimatized stepwise

153   to the low-strength (0.5 kgCOD.m^{-3}.d^{-1}) and psychrophilic temperature (25°C) for 20 months

154   before the beginning of this study. The total solids concentration in the G-AnMBR was 70–80

155   gTS.L^{-1}. No sludge was purged during the 357 days of the experiment except for sampling.

156   **2.2 Experimental design and operating conditions**

157   Four experimental periods were used to assess the impact of design parameters on G-AnMBR

158   performance, membrane fouling behavior and economic assessment. The influent flow was

159   progressively increased, with a direct impact on hydraulic retention time (HRT), organic

160   loading rate (OLR) and permeate flux (J_{20}). The G-AnMBR was then operated according to the

161   following conditions: instantaneous filtration fluxes ($J_{20,inst}$) of 2.8, 3.6, 4.1 and 6.0 LMH, HRT

162   from 14 to 5 h, and OLR from 0.5 to 1.6 kgCOD.m^{-3}.d^{-1} (Table 2), which are within the

163   common range of AnMBR studies for domestic WW treatment (Vinardell et al., 2020). The end

164   of each period was reached when a steady efficiency of COD removal was achieved and the

165   fouling rate was constant and considered to be sufficiently long to be representative of the

166   period. The maximal TMP recommended for the membrane supplier was 400–500 mbar.

Table 2 – G-AnMBR operating conditions during the different operating periods.

Parameters	Period 1	Period 2	Period 3	Period 4
Days of operation (d)	1–134	135–203	204–289	290–357
$Jp_{20,inst}$ (LMH)	2.8 ± 0.1	3.6 ± 0.1	4.1 ± 0.3	6.0 ± 1.4
$Jp_{20,net}$ (LMH)	1.3 ± 0.1	1.8 ± 0.1	2.5 ± 0.2	3.6 ± 1.2
HRT (h)	$13.9 \pm 0,5$	9.9 ± 0.3	7.0 ± 0.7	4.9 ± 1.4
OLR (kgCOD.m^{-3}.d^{-1})	0.5 ± 0.1	0.8 ± 0.2	1.0 ± 0.4	1.6 ± 0.7
Temperature (°C)	25.0 ± 0.3	25.0 ± 0.8	24.9 ± 1.2	25.3 ± 2.0
pH (–)	7.2 ± 0.6	7.0 ± 0.2	7.3 ± 0.2	7.4 ± 0.2
Redox (mV)	-488 ± 22	-488 ± 17	-494 ± 14	-478 ± 23
ULV (m.h^{-1})	2.6 ± 0.03	2.6 ± 0.03	2.6 ± 0.03	2.6 ± 0.03

168

2.3 Membrane fouling indicators

The extent of membrane fouling was evaluated through the monitoring of transmembrane pressure (TMP). A pressure gauge was installed on the permeate line, and data were recorded every 15 seconds. Data processing allowed calculation of the average maximal TMP per day.

Filtration resistance analysis was used to understand fouling mechanisms. Fouling resistance was measured using Darcy's law (Eq. 1) and the resistance-in-series model (Eq. 2).

$$R_t = \frac{TMP}{\mu_{20} \cdot J_{20}}$$

Eq. 1

$$R_t = R_m + R_f = R_m + (R_{reversible} + R_{irreversible} + R_{residual})$$

Eq. 2

where R_t is the resistance (m^{-1}), *TMP* is the transmembrane pressure (Pa), J_{20} is the normalized flux at 20°C (L.m^{-2}.h^{-1}), μ_{20} is the viscosity of water at 20°C (Pa.s), R_m is the membrane resistance (m^{-1}), R_f is the fouling resistance (m^{-1}) and $R_{reversible}$, $R_{irreversible}$ and $R_{residual}$ are the resistances caused by reversible fouling, irreversible fouling and residual fouling, respectively (m^{-1}).

180 All resistances were measured by filtering deionized water through the membrane. R_m was

181 measured with a clean membrane, R_t was measured at the end of experimental periods with a

182 fouled membrane and R_f was deduced. Subsequently, the fouled membrane was physically

183 cleaned by water rinsing with 5 L of deionized water allowing for calculation of $R_{reversible}$.

184 Finally, the membrane was chemically cleaned by soaking (2 h) in a 0.2% NaOCl solution,

185 providing the resistance removed by chemical cleaning $R_{irreversible}$ and the residual resistance

186 $R_{residual}$.

2.4 Analytical procedures

188 Influent, supernatant and effluent were sampled twice per week to measure the tCOD and sCOD

189 concentration using commercial kits (Hach, Germany, LCK 500, 314, 514). The supernatant

190 was sampled on the liquid recirculation line. The sCOD concentration was measured after pre-

191 filtration at 0.45μm. sCDO removal was divided into 'biological removal' and 'membrane

192 removal' (section 3.1.1). The sCOD removed between influent and supernatant was associated

193 to 'biological removal' whereas the sCOD removal measured between supernatant and

194 permeate was related to 'membrane removal'. It should be noticed that the 'membrane removal'

195 takes into account the membrane barrier rejection and the potential biological removal by the

196 biofilm developed on membrane surface. VFAs were analyzed regularly by ion-exclusion

197 chromatography (ICS-900, Dionex, USA; column BP-OA_2000, Benson Polymeric Inc., USA)

198 coupled with UV detector (210 nm). H_2SO_4 (0.05N) was used as eluent at 0.4 mL.min^{-1}. Six

199 VFAs were quantified, namely acetic acid, propionic acid, butyric acid, iso-butyric acid, iso-

200 valeric acid and valeric acid. All samples were passed through a 0.22 μm filter prior to HPLC-

201 UV analysis. Mixed liquor suspended solids were measured according to standard methods

202 (APHA et al., 1998).

203 A three-dimensional fluorescence excitation emission matrix (3DEEM) was used to

204 characterize the composition of the DCOM of the foulant. After physical cleaning, the collected

11

205   foulant was mixed thoroughly and pre-filtered through a 1.2 µm filter to conserve the colloidal

206   compounds. A fluorescence spectrophotometer (FL 6500, Perkin-Elmer, USA) was used with

207   excitation and emission scan ranges of 200–500 nm and 280–600 nm, respectively. Data

208   analysis was performed according the protocol of Jacquin et al. (2017). Three regions of

209   fluorophores were distinguished, namely (a) region I + II, associated with protein-*like*

210   molecules, (b) region IV, corresponding to soluble microbial product (SMP)-*like* molecules,

211   and (c) region III + V, related to humic substances.

212   Quantification of proteins (PN) and polysaccharides (PS) was conducted following the Lowry

213   and Dubois methods, respectively (Dubois et al., 1951; Lowry et al., 1951). Bovine serum

214   albumin (BSA) and glucose were used as standards. All samples were pre-filtered through a

215   0.45 µm filter before PN and PS quantification.

216   The extracellular polymeric substances (EPS) of the fouling layer were quantified because they

217   play a key role in membrane fouling. The EPS basically can be divided into three fractions

218   depending on their structure: soluble EPS, also known as soluble microbial products (SMPs),

219   loosely-bound EPS (LB-EPS) and tightly-bound EPS (TB-EPS). The heating extraction method

220   described by Li and Yang (2007) was used. The concentration of each EPS fraction was

221   quantified as the sum of PN and PS contents.

222   **2.5 COD mass balance**

223   The COD mass balance (gCOD.d^{-1}) was determined according to Eq. 3.

$$tCOD_{in} = tCOD_{out} + COD_{CH4}^{G} + COD_{CH4}^{L} + COD_{SO4} + \Delta COD_{biomass} \qquad \text{Eq. 3}$$

224   where $tCOD_{in}$ and $tCOD_{out}$ are the tCOD concentrations experimentally measured in the

225   influent and effluent (mg.L^{-1}), respectively; COD_{CH4}^{G} and COD_{CH4}^{L} are the equivalent COD

226   concentrations of the produced gaseous and dissolved methane, respectively; COD_{SO4}

227   corresponds to the COD used for the reduction of sulfate by sulfate-reducing bacteria (0.67

228 gCOD.gSO$_4^{-1}$); and $\Delta COD_{biomass}$ is the COD used for biomass synthesis (0.1 gVSS.gCOD^{-1}).

229 The dissolved methane (COD_{CH4}^{L}) was quantified experimentally following the headspace

230 method described by Sanchez et al. (2022). Total methane produced was calculated using the

231 theoretical value of 0.38 L-CH$_4$/gCOD$_{removed}$ at 25°C, allowing for the gaseous methane

232 (COD_{CH4}^{G}) calculation.

233 **2.6 Preliminary economic evaluation**

234 The economic assessment was conducted for four scenarios, corresponding to the four operating

235 periods. The design parameters, process performance and membrane fouling rates of the four

236 experimental periods were used for the calculations. The economic analysis was performed

237 considering a wastewater flow rate of 20,000 m^3.d^{-1} (i.e. 100,000 population equivalent).

238 Detailed information of the design criteria for each scenario can be found in Table A1 of the

239 supplementary data.

240 The capital and operating costs influenced by permeate flux, membrane fouling rate and process

241 performance were included in the economic evaluation. For this reason, the costs not influenced

242 by the evaluated parameters have not been included in the economic evaluation because they

243 are expected to be similar for the four scenarios. Capital expenditures (CAPEX) comprised the

244 purchase of the membranes, the bioreactor construction and the combined heat and power

245 (CHP) unit for biogas valorization. Operational expenditures (OPEX) comprised the chemical

246 reagents needed for membrane chemical cleaning, energy consumption for CHP unit and the

247 equipment replacement cost (i.e., membrane and CHP unit). Revenues corresponded to the

248 energy recovered from the biogas. All design and cost parameters used to calculate costs and

249 revenues are provided in Table A3 of the supplementary data.

250 The chemical cleaning protocol was adapted from Brepols et al. (2008) and used a 0.05%

251 NaOCl solution (2 h) and a 2,000 mg.L^{-1} citric acid solution (2 h). A chemical cleaning was

13

252 considered required when the maximal applicable TMP of 400 mbar was reached. It was

253 assumed that the initial membrane permeability was recovered after each chemical cleaning.

254 Chemical cleanings have an impact on membrane lifetime because the chemicals damage the

255 membrane materials and modify their properties and performance (Chheang et al., 2022). The

256 replacement of the membrane was presumed to be conducted when a maximum cumulative

257 chlorine contact of 500,000 mg.L^{-1}.h^{-1} was reached (Robles et al., 2014; Vinardell et al., 2022).

258 The present value of the net cost (PV$_{NC}$) was calculated for the four scenarios as the difference

259 between the PV of the gross cost (CAPEX + OPEX) and the PV of the electricity revenue

260 considering three plant lifetimes (i.e., 20, 30 and 40 years) and a discount rate of 5%. Detailed

261 information regarding the equations used for the economic evaluation can be found in Table

262 A3 of the supplementary data.

3. Results and discussion

3.1 Overall treatment performance

3.1.1 Biological and membrane rejection performances

266 Table 3 summarizes the average tCOD, VFA and MLSS values for the four periods. The tCOD

267 removal efficiency ranged between 82.5% and 92.6%, with average tCOD concentrations in the

268 effluent varying from 22.5 to 52.9 mgCOD.L^{-1}, which was in compliance with European Union

269 discharge standards (Directive 91/271/EEC). The MLSS in the permeate were below 5 mg.L^{-1}

270 in every experimental period, which was considerably below the 35 mgSS.L^{-1} regulation

271 discharge (Directive 91/271/EEC). The concentration of MLSS in the supernatant slightly

272 increased with the decrease of HRT (Pearson's correlation coefficient $r = -0.852$). This result

273 was expected because (i) ultrafiltration membranes retain particulate matter, which can

274 accumulate over time and (ii) lower HRT induces higher OLR, increasing levels of particulate

275 and colloidal materials and thus promoting biomass growth (R. Chen et al., 2017b; Huang et

276   al., 2011). Solid concentration build-up near the membrane has been previously correlated with

277   TMP increase (Gouveia et al., 2015).

278   Table 3 – Influent and effluent compositions and removal efficiencies (mean values ± SD; $n \geq 10$).

| Parameters	Units	Period 1	Period 2	Period 3	Period 4
OLR	kgCOD.m^{-3}.d^{-1}	0.5 ± 0.1	0.8 ± 0.2	1.0 ± 0.4	1.6 ± 0.7
tCOD$_{in}$	mgCOD/L	311.4 ± 54.7	346.4 ± 63.8	303.0 ± 91.0	298.8 ± 74.5
tCOD$_{eff}$ = sCOD$_{eff}$	mgCOD/L	22.5 ± 7.7	24.8 ± 7.4	32.7 ± 17.6	52.9 ± 28.4
tCOD$_{removal}$	%	92.4 ± 3.1	92.6 ± 2.2	89.1 ± 4.7	82.5 ± 7.7
VFA$_{inf}$	mgCOD/L	209.2 ± 43.2	159.2 ± 38.0	170.7 ± 10.0	190.3 ± 11.1
VFA$_{eff}$	mgCOD/L	0.0 ± 0.0	3.6 ± 4.6	2.3 ± 1.7	1.6 ± 2.2
VFA$_{removal}$	%	100 ± 0	97 ± 4	96 ± 5	99 ± 1
MLSS$_{supernatant}$	mg/L	88 ± 50	179 ± 108	209 ± 106	194 ± 99
MLSS$_{eff}$	mg/L	3.6 ± 3.9	1.3 ± 2.1	1.8 ± 0.7	3.8 ± 2.8

279

280   Fig. 1a presents the distribution of sCOD removal during the different periods. Under all

281   conditions, 10 ± 1.5% of the sCOD influent was removed by the physical membrane barrier

282   and/or by the biomass attached to the membrane surface. This highlights that the effectiveness

283   of membrane separation was not affected by the filtration flux. The retention of particulate

284   matter and some DCOM by the membrane was observed to improve effluent quality further and

285   enhance the removal rate of organic material (Gouveia et al., 2015; Sanchez et al., 2022; Smith

286   et al., 2013). No statistical difference was observed among the tCOD removal efficiencies

287   achieved in all experimental periods ($p > 0.05$) with the exception of Period 4.0 ($p < 0.05$). In

288   this latter case, when the OLR increased from 1.0 to 1.6 kgCOD.m^{-3}.d^{-1}, biological sCOD

289   removal dropped to 57%. The G-AnMBR performances rose progressively for 45 days until

290   reaching an average biological sCOD removal of 80.6 ± 5.5 and a tCOD removal rate of 92.7

291   ± 1.5%. Thus, the anaerobic microbial community eventually adapted to harsh operational

292   conditions, probably due to membrane retention that uncoupled HRT and SRT and thus allowed

293   for acclimation of anaerobic bacteria and archaea (Stuckey, 2012). These results are consistent

294 with those obtained by Ji et al. (2021), who operated a submerged AnMBR for domestic

295 wastewater treatment at 25°C under different operating conditions. For an OLR between 1.5

296 and 0.7 kgCOD.m^{-3}.d^{-1} (HRT 6–12 h), a steady high COD removal efficiency above 89% was

297 observed. However, the biological performance substantially decreased at an OLR of 2.1

298 kgCOD.m^{-3}.d^{-1} (HRT 4h), although the organic material retained by the membrane

299 compensated for the decrease in bioactivity (Ji et al., 2021a).

300 Fig. 1b shows the VFA concentrations measured in the influent, supernatant and effluent of the

301 G-AnMBR. The VFA concentration is expressed as the sum of all VFAs converted into COD

302 equivalents. Among the VFAs analyzed, acetic acid and propionic acid were the predominant

303 compounds (10–120 mg/L); butyric acid, iso-butyric acid and iso-valeric acid were near the

304 limit of quantification (<2 mg.L^{-1}); and valeric acid was below the level of detection (<0.5

305 mg.L^{-1}). VFAs are key intermediate products of anaerobic digestion and their concentrations

306 within the mixed liquor give an indication about the process stability and the proper functioning

307 of methane-producing archaea (van Lier et al., 2008). The lower the amount of VFA, the more

308 efficient the anaerobic reaction chain. Low amounts of VFAs were measured, and no VFA

309 accumulation was observed in the G-AnMBR supernatant during the experimental periods. This

310 analysis confirms that (i) a steady state was reached and (ii) the anaerobic bacteria and archaea

311 were consistent with all the conditions evaluated. Furthermore, Fig. 1b reveals very low VFA

312 concentration in the permeate (1.9 ± 1.3 mgCOD.L^{-1}), revealing that these compounds were

313 biologically degraded and additionally removed in the membrane separation step (Fig. 1b).

314 Theoretically, VFAs could pass through the membrane due to their low molecular weight but

315 this phenomenon has been previously observed, demonstrating the positive impact of fouling

316 layer biological activity (Chen et al., 2017a; Martinez-Sosa et al., 2011). Previous studies have

317 hypothesized that the biomass attached to membrane surface is considerably active, even more

318 active than suspended biomass, because of lower mass-transfer limitations (Smith et al., 2013).

319
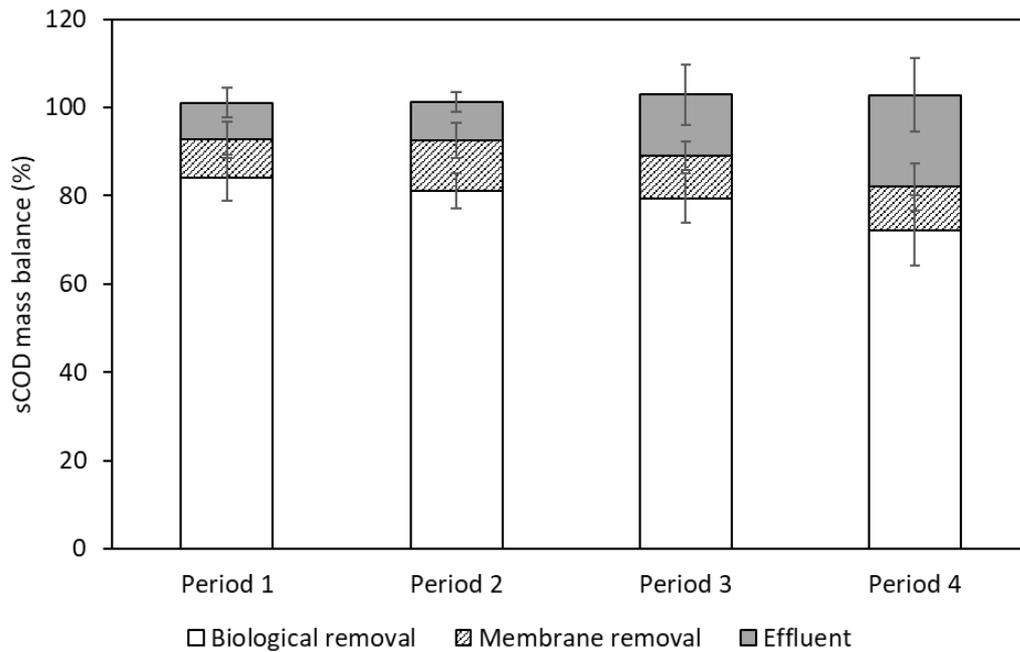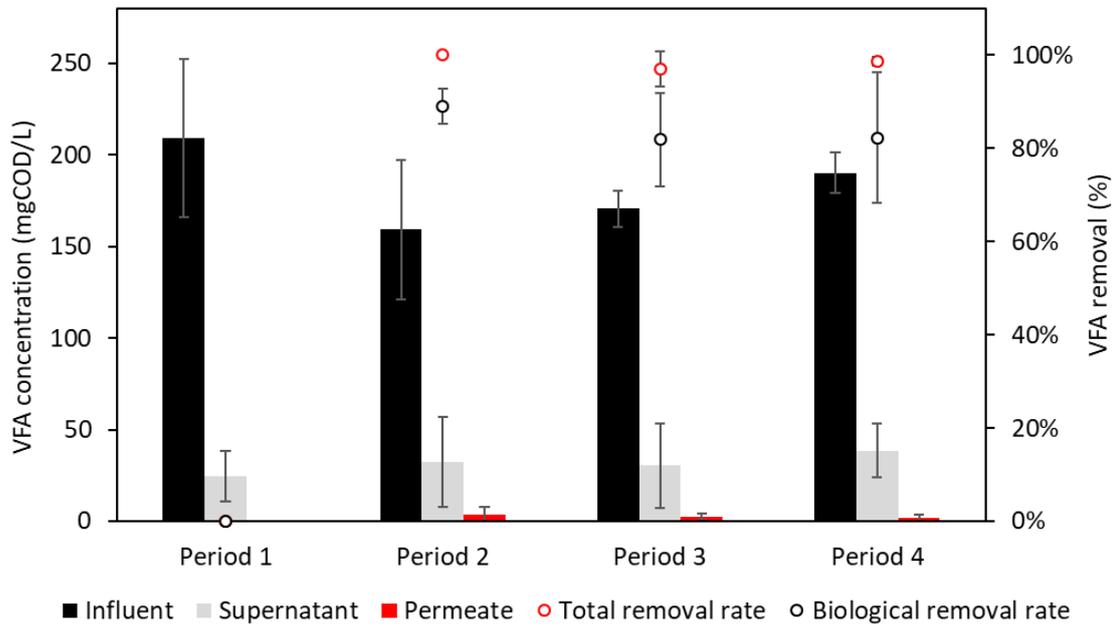
Fig. 1 – (a) Distribution of sCOD biological removal, membrane removal and effluent content; (b) VFA
concentration and removal efficiency under all operating conditions (HRT 14, 10, 7, 5 h; OLR 0.5, 0.8, 1.0, 1.6
kgCOD.m^{-3}.d^{-1} for periods 1, 2, 3 and 4, respectively).

3.1.2 COD mass balance

COD mass balance distribution for the four operational conditions is provided in Table 4. The

COD contained in the effluent and the methane production were the two major factors affected

by the changes in OLR. As expected, the quantity of COD_{in} converted into methane increased

327   considerably, from 2.7 to 7.4 gCOD.d^{-1} (2.7-fold), and the influent flux increased from 3.55 to

328   10.70 gCOD.d^{-1} (3-fold). However, the fraction of the tCOD converted into methane decreased

329   from 77% to 70% as the OLR increased from 0.5 to 1.6 kg.m^{-3}.d^{-1}, respectively. At the same

330   time, the proportion of COD$_{in}$ retrieved as dissolved methane (lost methane) decreased from

331   27% to 10% when the OLR increased (Table 4). These results indicate that a trade-off must be

332   found in the applied operating conditions to enable both a high rate of conversion of organic

333   matter to methane and a lower concentration of dissolved methane.

334   Dissolved methane measured during the periods was lower as OLR increased (r = −0.95).

335   Specifically, dissolved methane concentration was 21.2 ± 1.3 mg.L^{-1} for Period 1, 20.5 ± 2.4

336   mg.L^{-1} for Period 2, 14.7 ± 2.1 mg.L^{-1} for Period 3 and 9.3 ± 3.0 mg.L^{-1} for Period 4. Similarly

337   to the present study, Yeo et al. (2015) observed that the fraction of dissolved methane (relative

338   to the total methane produced) decreased from 35 to 14% as the OLR increased from 0.4 to 1.1

339   kgCOD.m^{-3}.d^{-1}. The increase in gas production at higher OLR levels led to an increase in local

340   turbulence and mass transfer, allowing more methane to escape the liquid phase and

341   diminishing the level of supersaturation (Yeo et al., 2015).

342   Table 4 – COD mass balance during each experimental period.

Period	1		2		3		4	
	gCOD.d^{-1}	%	gCOD.d^{-1}	%	gCOD.d^{-1}	%	gCOD.d^{-1}	%
Influent COD	**3.55**	**100**	**5.50**	**100**	**7.10**	**100**	**10.70**	**100**
Effluent COD	0.27	8	0.41	7	0.83	12	1.74	16
Sludge growth	0.47	13	0.72	13	0.89	13	1.27	12
Sulfate reduction	0.10	3	0.16	3	0.20	3	0.28	3
Dissolved CH$_4$	0.95	27	1.34	24	1.37	19	1.04	10
Gaseous CH$_4$	1.77	50	2.86	52	3.82	54	6.37	60
Total CH$_4$	2.72	77	4.20	76	5.19	73	7.41	70

343

3.2 Membrane fouling behavior

3.3.1 Membrane filtration performance

Fig. 2 shows the extent of membrane fouling through the TMP evolution along the operational periods. Table 5 provides the membrane fouling rates obtained from the TMP profiles. Substantial differences in TMP profiles were observed between each period. During Period 1 ($Jp_{20,net}$ = 2.8 LMH), TMP slowly increased to 46 mbar with a progressive rise of 0.03 kPa.d^{-1} (Table 5). The very low membrane fouling rate suggests that the membrane was operating at sub-critical filtration flux, as no severe fouling was observed. When the instantaneous filtration flux was increased to 3.6 LMH (Period 2), the TMP reached 305 mbar (ΔTMP = 236 mbar) after 65 days of filtration. The TMP profile was characterized by a slow upward trend (0.16 kPa.d^{-1}), followed by a much faster fouling rate (0.87 kPa.d^{-1}), resulting in an average fouling rate estimated at approximately 0.40 kPa.d^{-1} (Table 5). In Period 3 ($Jp_{20,inst}$ = 4.1 LMH), TMP rapidly and steadily increased, with an average daily rise of 0.65 kPa.d^{-1}, until a maximal TMP of 430 mbar was reached. During Period 4, the initial filtration flux targeted ($Jp_{20,inst}$ = 7.5 LMH) led to very strong and fast membrane fouling; the average instantaneous flux in this period was of 6.0 ± 1.4 LMH. The TMP increased from 40 mbar to 530 mbar within 9 days (day 290 to 299), and constant instantaneous filtration flux was unable to be sustained, thus decreasing slowly to 5.7 LMH. On day 303, the membrane was removed from the reactor for physical and chemical cleaning. The filtration for Period 4 was restarted, and the same sharp upward trend in TMP was observed after the membrane cleaning. The membrane fouling rate was approximately 2.86 kPa.d^{-1}. On day 316, the maximal TMP was reached; then, the instantaneous permeate flux dropped progressively to 4.1 LMH until the end of the experiment. The concept of critical flux states that under fixed operating conditions (e.g., MLSS, hydrodynamics conditions, membrane properties) there is a threshold flux above which a sustainable flux cannot be further maintained (Bacchin et al., 2006). Fig. 2 clearly shows that

19

369 apart from Period 1 ($Jp_{20,inst}$ = 2.8 LMH), the critical flux was exceeded because apparent

370 fouling was observed during the experimental periods. Conversely, a critical instantaneous flux

371 of 5 LMH was obtained in a mesophilic (30°C) AnMBR at a TSS concentration of 50 g.L^{-1}

372 when gas sparging (U_g = 35 m/h) was applied (Jeison and van Lier, 2006). The lower critical

373 flux obtained in this study can be attributed to the very high concentration of solids and the

374 poor shear rate due to the absence of gas sparging.

375 These results confirm that the TMP substantially increased with the permeate flux, which

376 confirms the high impact of permeate flux on membrane fouling. The increase in filtration flux

377 led to higher convective forces in such a way that foulants were pushed toward the membrane

378 surface more harshly and quickly; thus, the lift and diffusion forces had less effect in carrying

379 foulants away (Chen et al., 2017a).

380 Table 5 – Fouling rates at different filtration conditions.

Period	Filtration conditions	Fouling rates	
	$Jp_{20,inst}$ (LMH)	$dTMP/dt$ (kPa.d^{-1})	dR/dt (m^{-1}.d^{-1})
1	2.8 ± 0.1	0.03	0.9×10^{11}
2	3.6 ± 0.1	0.40	9.3×10^{11}
3	4.1 ± 0.3	0.65	10.3×10^{11}
4	6.0 ± 1.4	2.86	34.0×10^{11}

381
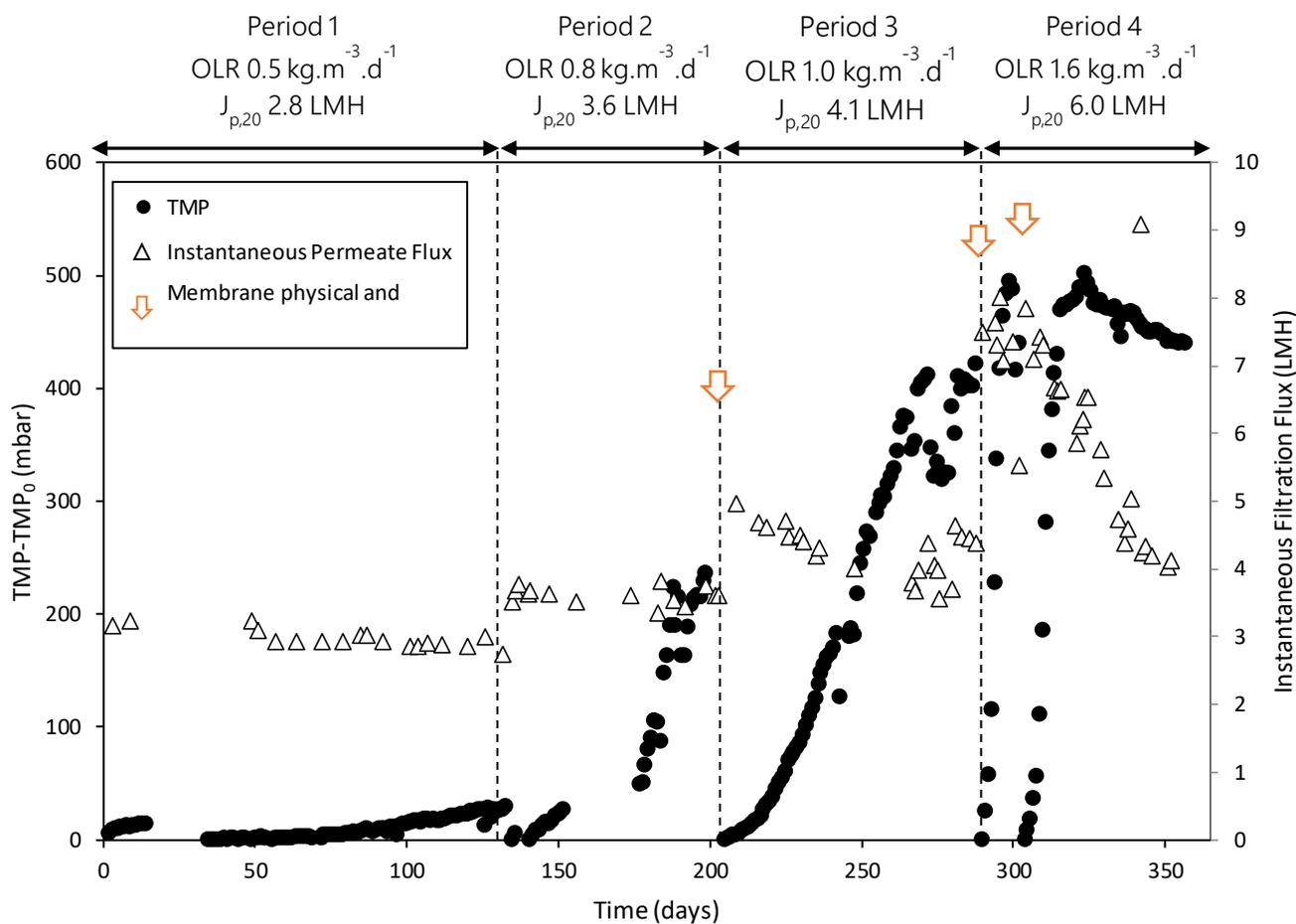
Fig. 2 – Transmembrane pressure and instantaneous filtration flux during the operational periods.

3.3.2 Membrane fouling resistances

The extent of reversibility of the fouling layer was evaluated based on the distribution of the fouling resistances (Table 6). Because the fouling rate in Period 1 was very low (Table 5) and the TMP on day 134 was approximately 50 mbar, no membrane cleaning was performed between Period 1 and Period 2. Therefore, no membrane fouling resistance distribution is available for Period 1. Fouling resistance (R_f) corresponded to $15.0 \pm 1.1 \times 10^{12}$, $16.8 \pm 0.6 \times 10^{12}$ and $25.7 \pm 4.7 \times 10^{12}$ m^{-1} for periods 2, 3 and 4, respectively. These results demonstrate that R_f was strongly correlated to permeate flux and OLR ($r > 0.99$, $p < 0.05$). $R_{reversible}$ accounted for 100%, 97.9% and 97.7% of the membrane fouling resistance, indicating that fouling was mostly reversible under all the operating conditions tested. External deposition, especially in the cake layer, was the main mechanism involved in G-AnMBR fouling, in

21

395 agreement with previous studies (Anjum et al., 2021; Kaya et al., 2017; Lin et al., 2013). Only

396 residual fouling of $0.1 \pm 0.0 \times 10^{12}$ and $0.2 \pm 0.1 \times 10^{12}$ m^{-1} were measured for periods 3 and

397 4. High filtration fluxes have been observed to promote the extent of intermediate pore blocking

398 in the early filtration step, which may lead to more severe or resistant fouling (Lin et al., 2013;

399 Yao et al., 2022). However, the contribution of residual fouling to the total resistance was minor

400 in comparison to the clean membrane ($R_m = 0.8 \pm 0.1 \times 10^{12}$ m^{-1}).

401 These results are promising for mitigation of G-AnMBR fouling, suggesting that a well-

402 designed backwash (i.e., physical cleaning) could lead to longer filtration performance. Further

403 research is needed to optimize the backwash parameters, such as intensity, frequency and

404 duration, for the purpose of developing sustainable G-AnMBR domestic wastewater treatment.

405 Table 6 – Fouling resistance distribution for experimental periods 2, 3 and 4.

Resistances	Units	Period 2	Period 3	Period 4
$R_{fouling}$	$\times 10^{12}$ m^{-1}	15.0 ± 1.1 (100%)	16.8 ± 0.6 (100%)	25.7 ± 4.7 (100%)
$R_{reversible}$	$\times 10^{12}$ m^{-1}	15.0 ± 1.1 (100%)	16.4 ± 0.7 (97.9%)	25.1 ± 4.6 (97.7%)
$R_{irreversible}$	$\times 10^{12}$ m^{-1}	–	0.3 ± 0.1 (1.9%)	0.4 ± 0.1 (1.6%)
$R_{residual}$	$\times 10^{12}$ m^{-1}	–	0.1 ± 0.0 (0.2%)	0.2 ± 0.1 (0.8%)

406

407 3.3.3 Membrane foulants characteristization

408 The composition of the reversible fouling was characterized through 3DEEM analysis (Fig. 3a),

409 while the 3DEEM content of mixed liquor and permeate have been analyzed and published in

410 previously published study (Sanchez et al., 2022). Based on previous works, three regions of

411 fluorophores were distinguished, namely (a) region I + II, associated with protein-like

412 molecules, (b) region IV, corresponding to soluble microbial product (SMP)-like molecules,

413 and (c) region III + V, related to humic substances (Chen et al., 2003; Jacquin et al., 2017) (see

414 Fig. A2). Since polysaccharides are not analyzed through fluorescence excitation emission,

22

415   additional foulant characterization were performed through PN and PS quantification (Fig. 3b).

416   Among the three fluorescent regions investigated, the major volume of fluorescence belonged

417   to region I + II (72–85%), relating to colloidal and macromolecular protein-*like* compounds

418   (Jacquin et al., 2017). In addition, between 11% and 20% of the total fluorescence volume was

419   part of region III + V, corresponding to humic substances. Measurement of PN and PS contents,

420   presented in Fig. 3b, corroborates the predominance of PN materials within the fouling layer,

421   with proportions of PN approximately 55%, 77% and 84% for periods 2, 3 and 4, respectively.

422   It can therefore be assumed that PN in the form of colloidal materials and macromolecules

423   prevailed in the G-AnMBR foulant, in accordance with previous observations (R. Chen et al.,

424   2017a; Yao et al., 2020; Zhou et al., 2016). The PN to PS ratio (PN/PS) was found to be strongly

425   correlated with the decrease in HRT ($r = -0.996$, $p < 0.05$), demonstrating the rise in PN

426   concentration in the cake layer during the experimental periods. Several factors, including the

427   following, may be responsible for this phenomenon: (i) the increase of the permeate flux leads

428   to higher OLRs, which promote the growth of biomass and biopolymers (mainly composed of

429   PN and PS) (Huang et al., 2011); (ii) the decrease of HRT reduces degradation of polymers and

430   macromolecules because PN-based organic matter has been found to be more slowly and

431   weakly biodegradable than that based on PS, thus leading to PN accumulation (R. Chen et al.,

432   2017a; Yang et al., 2015); and (iii) PN has been reported to have higher hydrophobic

433   characteristics than PS. Accordingly, PN has more tendency to adhere to membrane surface

434   (Kaya et al., 2019).

435   Because EPS have been identified as a key factor in membrane fouling (Anjum et al., 2021; R.

436   Chen et al., 2017a; Ding et al., 2015), the fouling layer was further fractionated into SMP, LB-

437   EPS and TB-EPS to identify the contribution of EPS fractions to total fouling. Fig. 3c shows

438   the repartition of the three EPS fractions extracted from the cake layer in periods 2, 3 and 4. Of

439   the three EPS fractions, the TB-EPS were in higher proportion within the fouling layer for all

440 the periods, followed by the SMP content and LB-EPS content. Nonetheless, the TB-EPS

441 content progressively decreased from 63% to 43% as the permeate flux increased from 1.8 to

442 3.6 LMH, respectively. Conversely, the fraction of SMPs extracted from the fouling layer

443 increased from 9% to 31% with the increase of permeate flux. The increase in SMPs was

444 probably caused by the OLR increase and HRT decrease, which stimulated production of SMPs

445 and reduced their degradation (Huang et al., 2011).

446 On the one hand, it might be concluded that bound-EPS (TB- and LB-EPS) represented an

447 important fraction of the foulants deposit because bound-EPS were mostly within the fouling

448 layer, in agreement with previous studies (R. Chen et al., 2017a; Gao et al., 2011). On the other

449 hand, the SMP fraction increased with the increase of filtration flux and fouling resistance,

450 which could suggest that SMPs play an important role in membrane fouling. Ding et al. (2015)

451 studied the extent of fouling caused by the three EPS fractions extracted from the cake sludge

452 of a mesophilic AnMBR. It was found that at the same TOC concentration, SMPs caused the

453 highest filtration resistance (50.2%) followed by LB-EPS (19.8%) and TB-EPS (30.0%). It was

454 suggested that the SMP fraction exhibited a lower energy barrier than the bound-EPS fractions,

455 so that SMPs needed to overcome weaker repulsive interaction energy to adhere to the

456 membrane surface (Ding et al., 2015). Accordingly, it is important to consider both the relative

457 contribution and specific fouling resistance when evaluating the impact of EPS fractions (i.e.,

458 SMP, LB-EPS, TB-EPS) on membrane fouling. Although no clear conclusion can be provided

459 regarding the major EPS contributor, the abundance of bound-EPS indicated the presence of

460 biomass attachment on the membrane surface, while the SMP revealed an implication of

461 dissolved compounds in global membrane fouling. Therefore, it is possible to conclude that the

462 fouling was mainly due to the combination of organic and biological fouling.

463 To summarize, fouling layer analysis indicated that PN materials were the main foulant in the

464 G-AnMBR system that was studied. PN content was highly influenced by the operating

465   conditions. EPS clearly played a relevant role in membrane fouling. The role of EPS fractions

466   in membrane fouling is still not clear; however, it is hypothesized that they can (i) participate

467   in biomass–membrane bonding (bound-EPS), (ii) form a strong interaction with the membrane

468   surface (SMPs) and (iii) create a wide EPS network, consolidating the cake layer.

(a)

(b)

(c)

469
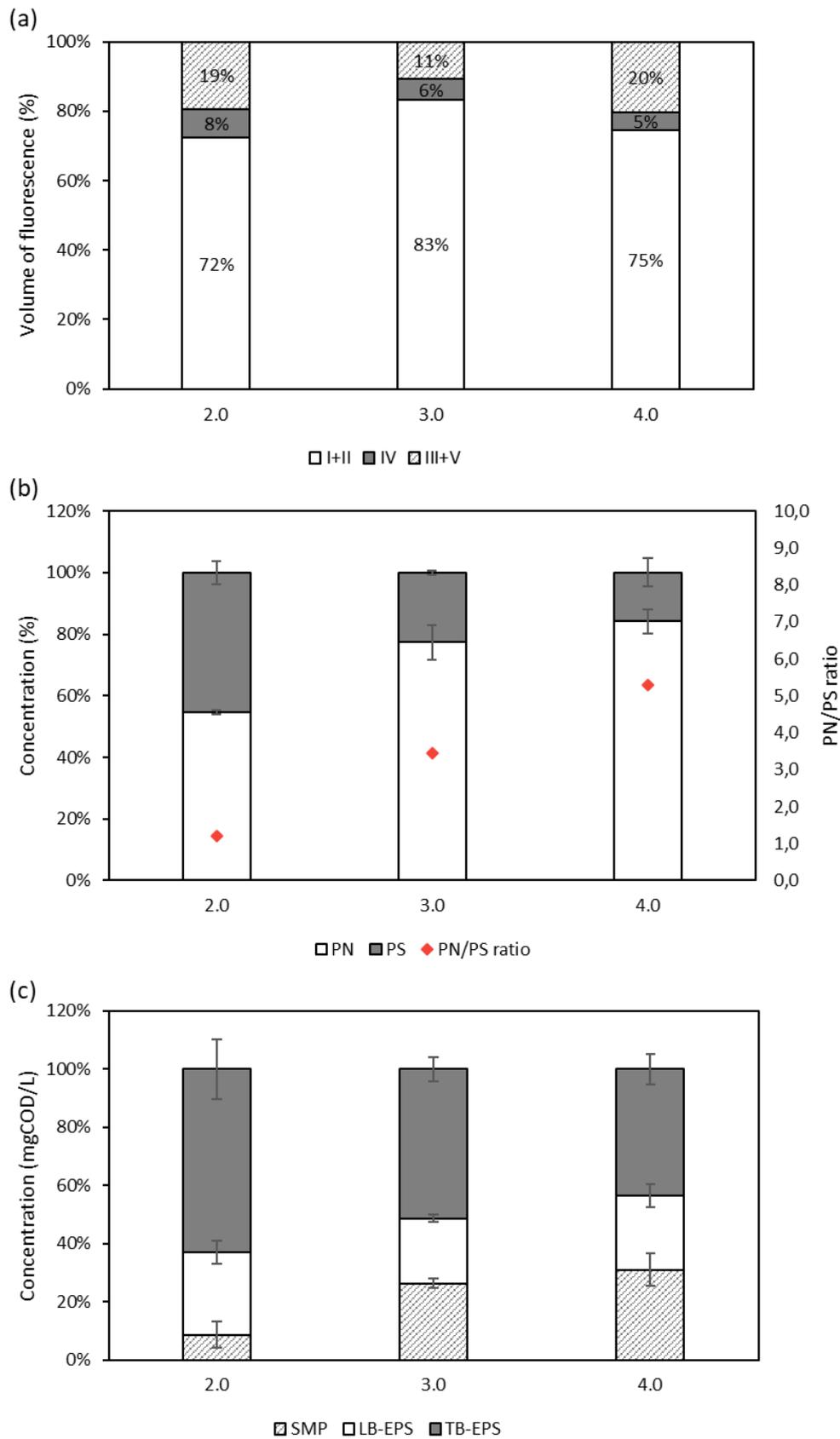
Fig. 3 – Composition of membrane foulants obtained through (a) 3DEEM (I + II: protein-*like* substances, III + V: humic-*like* substances, IV: SMP-*like* molecules); (b) PN and PS concentration; (c) EPS concentration.

3.3 Preliminary economic evaluation

472

473 Fig. 4a shows the gross cost, electricity revenue and net cost for the four scenarios evaluated

474 for a plant lifetime of 30 years. Fig. A3 and A4 of the supplementary information illustrate the

475 same results for a plant lifetime of 20 and 40 years, respectively. The results show that scenarios

476 3 and 4 featured the lowest net cost for the G-AnMBR system under study. The lower net cost

477 of these scenarios compared with scenarios 1 and 2 can be mainly attributed to the lower

478 membrane area required. This effect indicates that operating the membrane system at $J_{20,inst}$

479 below 3.6 LMH is not economically competitive for a G-AnMBR system operated without gas

480 sparging. Of note, the net cost of Scenario 3 ($Jp_{20,inst}$ 4.1 LMH) was slightly lower than Scenario

481 4 (6.0 LMH) (Fig. 4a). In Scenario 4, high amounts of chemicals were needed for membrane

482 cleaning (due to the high fouling rate) with a direct impact on membrane replacement

483 frequency. In this regard, the extra costs regarding membrane cleaning and replacement in

484 Scenario 4 did not offset the lower membrane purchase costs when compared with Scenario 3.

485 Accordingly, it is important to achieve a compromise solution between operating the

486 membranes at relatively higher fluxes (CAPEX) while consuming a moderate amount of

487 chemicals (OPEX). In this regard, further pilot- and demonstration-scale studies are necessary

488 to determine, at larger scale, the optimum flux and chemical cleaning conditions to reduce the

489 costs and improve the economic competitiveness of the G-AnMBR system. Besides cost

490 considerations, the operation of the G-AnMBR operated without gas sparging has the potential

491 to make the WWTP energy positive due to the biogas (60-70% CH_4) produced in the system

492 (0.4-0.5 $kWh \cdot m^{-3}$).

493 Fig. 4b shows the gross cost distribution for the different scenarios. Detailed information

494 regarding the distribution of the gross costs can be found in Table A4 of the supplementary

495 information. Membrane purchase accounted for more than 49% of the gross cost for all the

496 scenarios, although its contribution progressively decreased from 89% to 49% as the permeate

flux increased from 2.8 to 6.0 LMH, respectively. The chemical cleaning also featured a relatively important impact on the gross cost in scenarios 2, 3 and 4. The contribution of chemical cleaning sharply increased from 0.5 to 26.0% as the permeate flux increased from 2.8 to 6.0 LMH, respectively, because the extent of membrane fouling was substantially higher at higher fluxes. This was particularly important in Scenario 4, in which the high fouling rate and chemical cleaning frequency made replacement of the membrane system necessary during the plant's lifetime, with a direct impact on the OPEX (see Table A4 of the supplementary information). This highlights that the membrane chemical cleaning strategy is a key economic driver, especially in those scenarios in which intensive chemical cleaning is needed to control long-term membrane fouling. Figure 4b also shows that the bioreactor construction contribution decreased from 7.1 to 3.8% as the OLR increased from 0.5 to 1.6 kgCOD m^{-3} d^{-1}, respectively. This illustrates that increasing OLR has also an impact on the economic balance of the system. Overall, these economic results further corroborate that achieving a trade-off between increasing the flux and OLR (system intensification) without requiring intensive physical and chemical cleaning strategies to control membrane fouling is important for the economics of a G-AnMBR system operated in submerged mode and without gas sparging.

513
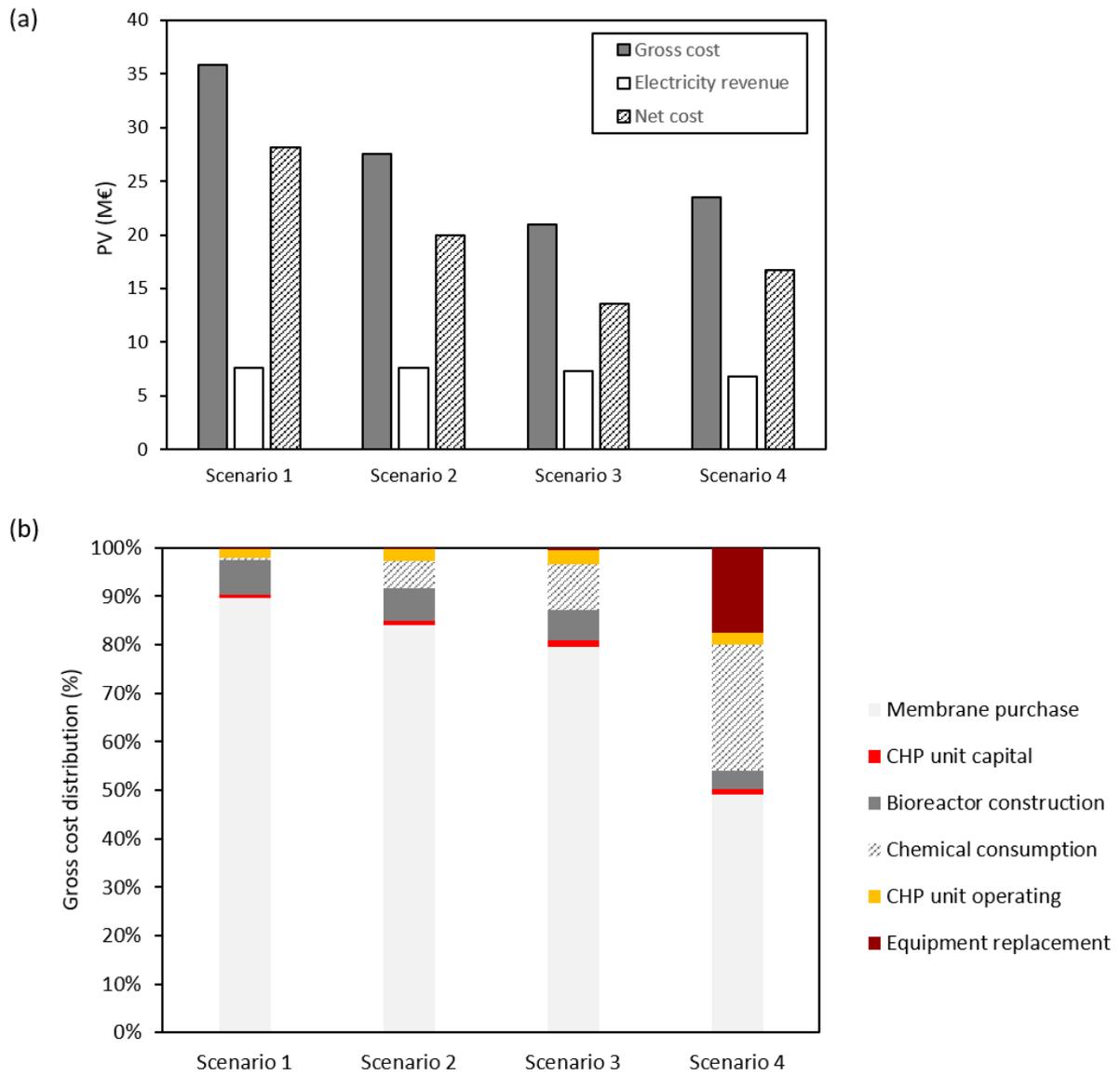
Fig. 4 – (a) Present value (PV) of the net cost, gross cost and electricity revenue; (b) gross cost distribution for
the four scenarios evaluated for a 30-year plant lifetime.

516

517

4. Conclusions

The present work studied the impact of design parameters (i.e., OLR, permeate flux, HRT) on a G-AnMBR operated with a submerged UF membrane and without gas sparging as fouling control for mainstream domestic wastewater at ambient temperature. Four design OLRs were tested (between 0.5 and 1.6 $kgCOD.m^{-3}.d^{-1}$) resulting in four HRT and permeate flux conditions.

- The G-AnMBR achieved a rapid steady-state and high COD removal efficiencies (>90%) for HRTs ranging between 14 and 7 h.

- The proportion of tCOD converted into methane was 77% at the lowest OLR and 70% at the highest OLR, confirming the decrease in biological activity with increasing OLR. However, more methane was recovered in the gaseous phase at the highest OLR (86% of the total methane produced) in comparison to the lowest OLR (65% of the total methane produced). Hence, at higher OLRs, the amount of bio-methane energy lost in the effluent and the greenhouse gas emissions were lowered.

- Membrane fouling increased with the permeate flux and OLR, highlighting the important role of those parameters in cake layer formation and build-up. Under all conditions, proteinaceous colloidal and macromolecules were the main components of the G-AnMBR cake layer. Membrane permeability was almost totally recovered after physical cleaning with water rinsing, demonstrating that fouling was mainly reversible.

- Finally, the economic evaluation showed that filtration flux, and the resulting membrane surface area, is a crucial parameter for G-AnMBR economics, with Scenario 3 (4.1 LMH) being the most economically favorable option.

540   Overall, these results have shown that achieving a compromise solution considering

541   permeate flux, OLR and chemical cleaning for membrane fouling control is important to

542   reduce the net cost of G-AnMBR systems operated without gas sparging.

543   On this basis, the G-AnMBR could be a sustainable and efficient process for domestic

544   wastewater treatment for local applications in which important financial, technical and

545   energy resources cannot be deployed.

Supplementary information

547 E-supplementary data for this work can be found in the e-version of this paper online.

Acknowledgments

552

553

References

554 **References**

555 Anjum, F., Khan, I.M., Kim, J., Aslam, M., Blandin, G., Heran, M., Lesage, G., 2021. Trends
556   and progress in AnMBR for domestic wastewater treatment and their impacts on process
557   efficiency and membrane fouling. Environmental Technology & Innovation 21,
558   101204. https://doi.org/10.1016/j.eti.2020.101204
559 APHA, AWWA, WEF (Eds.), 1998. Standard methods: for the examination of water and
560   wastewater, 20. ed. ed. American Public Health Association, Washington, DC.
561 Aslam, A., Khan, S.J., Shahzad, H.M.A., 2022. Anaerobic membrane bioreactors (AnMBRs)
562   for municipal wastewater treatment- potential benefits, constraints, and future
563   perspectives: An updated review. Science of The Total Environment 802, 149612.
564   https://doi.org/10.1016/j.scitotenv.2021.149612
565 Aslam, M., Charfi, A., Lesage, G., Heran, M., Kim, J., 2017. Membrane bioreactors for
566   wastewater treatment: A review of mechanical cleaning by scouring agents to control
567   membrane fouling. Chemical Engineering Journal 307, 897–913.
568   https://doi.org/10.1016/j.cej.2016.08.144
569 Bacchin, P., Aimar, P., Field, R.W., 2006. Critical and sustainable fluxes: Theory, experiments
570   and applications. Journal of Membrane Science 281, 42–69.
571   https://doi.org/10.1016/j.memsci.2006.04.014
572 Batstone, D.J., Virdis, B., 2014. The role of anaerobic digestion in the emerging energy
573   economy. Current Opinion in Biotechnology, Energy biotechnology • Environmental
574   biotechnology 27, 142–149. https://doi.org/10.1016/j.copbio.2014.01.013
575 Boulenger, P., Gallouin, Y., 2009. Traitements biologiques anaérobies des effluents industriels.
576   Ed. Techniques Ingénieur.
577 Brepols, C., Drensla, K., Janot, A., Trimborn, M., Engelhardt, N., 2008. Strategies for chemical
578   cleaning in large scale membrane bioreactors. Water Science and Technology 57, 457–
579   463. https://doi.org/10.2166/wst.2008.112
580 Chen, C., Guo, W., Ngo, H.H., Chang, S.W., Duc Nguyen, D., Dan Nguyen, P., Bui, X.T., Wu,
581   Y., 2017a. Impact of reactor configurations on the performance of a granular anaerobic
582   membrane bioreactor for municipal wastewater treatment. International
583   Biodeterioration & Biodegradation 121, 131–138.
584   https://doi.org/10.1016/j.ibiod.2017.03.021
585 Chen, C., Guo, W.S., Ngo, H.H., Liu, Y., Du, B., Wei, Q., Wei, D., Nguyen, D.D., Chang,
586   S.W., 2017b. Evaluation of a sponge assisted-granular anaerobic membrane bioreactor
587   (SG-AnMBR) for municipal wastewater treatment. Renewable Energy 111, 620–627.
588   https://doi.org/10.1016/j.renene.2017.04.055
589 Chen, R., Nie, Y., Hu, Y., Miao, R., Utashiro, T., Li, Q., Xu, M., Li, Y.-Y., 2017a. Fouling
590   behaviour of soluble microbial products and extracellular polymeric substances in a
591   submerged anaerobic membrane bioreactor treating low-strength wastewater at room
592   temperature. Journal of Membrane Science 531, 1–9.
593   https://doi.org/10.1016/j.memsci.2017.02.046
594 Chen, R., Nie, Y., Ji, J., Utashiro, T., Li, Q., Komori, D., Li, Y., 2017b. Submerged anaerobic
595   membrane bioreactor (SAnMBR) performance on sewage treatment: removal
596   efficiencies, biogas production and membrane fouling. Water science and technology
597   76, 1308–1317. https://doi.org/10.2166/wst.2017.240
598 Chen, W., Westerhoff, P., Leenheer, J.A., Booksh, K., 2003. Fluorescence Excitation−Emission
599   Matrix Regional Integration to Quantify Spectra for Dissolved Organic Matter. Environ.
600   Sci. Technol. 37, 5701–5710. https://doi.org/10.1021/es034354c
601 Chheang, M., Hongprasith, N., Ratanatawanate, C., Lohwacharin, J., 2022. Effects of Chemical
602   Cleaning on the Ageing of Polyvinylidene Fluoride Microfiltration and Ultrafiltration

Membranes Fouled with Organic and Inorganic Matter. Membranes (Basel) 12, 280. https://doi.org/10.3390/membranes12030280

Ding, Y., Tian, Y., Li, Z., Zuo, W., Zhang, J., 2015. A comprehensive study into fouling properties of extracellular polymeric substance (EPS) extracted from bulk sludge and cake sludge in a mesophilic anaerobic membrane bioreactor. Bioresource Technology 192, 105–114. https://doi.org/10.1016/j.biortech.2015.05.067

Dong, Q., Parker, W., Dagnew, M., 2016a. Influence of SRT and HRT on Bioprocess Performance in Anaerobic Membrane Bioreactors Treating Municipal Wastewater. Water Environment Research 88, 158–167. https://doi.org/10.2175/106143016X14504669767175

Dong, Q., Parker, W., Dagnew, M., 2016b. Long term performance of membranes in an anaerobic membrane bioreactor treating municipal wastewater. Chemosphere 144, 249–256. https://doi.org/10.1016/j.chemosphere.2015.08.077

Dubois, M., Gilles, K., Hamilton, J.K., Rebers, P.A., Smith, F., 1951. A Colorimetric Method for the Determination of Sugars. Nature 168, 167–167. https://doi.org/10.1038/168167a0

Evans, P.J., Parameswaran, P., Lim, K., Bae, J., Shin, C., Ho, J., McCarty, P.L., 2019. A comparative pilot-scale evaluation of gas-sparged and granular activated carbon-fluidized anaerobic membrane bioreactors for domestic wastewater treatment. Bioresource Technology 288, 120949. https://doi.org/10.1016/j.biortech.2019.01.072

Gao, W.J., Lin, H.J., Leung, K.T., Schraft, H., Liao, B.Q., 2011. Structure of cake layer in a submerged anaerobic membrane bioreactor. Journal of Membrane Science 374, 110–120. https://doi.org/10.1016/j.memsci.2011.03.019

Gouveia, J., Plaza, F., Garralon, G., Fdz-Polanco, F., Peña, M., 2015. A novel configuration for an anaerobic submerged membrane bioreactor (AnSMBR). Long-term treatment of municipal wastewater under psychrophilic conditions. Bioresource Technology 198, 510–519. https://doi.org/10.1016/j.biortech.2015.09.039

Hu, Y., Yang, Y., Yu, S., Wang, X.C., Tang, J., 2018. Psychrophilic anaerobic dynamic membrane bioreactor for domestic wastewater treatment: Effects of organic loading and sludge recycling. Bioresource Technology 270, 62–69. https://doi.org/10.1016/j.biortech.2018.08.128

Huang, Z., Ong, S.L., Ng, H.Y., 2011. Submerged anaerobic membrane bioreactor for low-strength wastewater treatment: Effect of HRT and SRT on treatment performance and membrane fouling. Water Research 45, 705–713. https://doi.org/10.1016/j.watres.2010.08.035

Jacquin, C., Lesage, G., Traber, J., Pronk, W., Heran, M., 2017. Three-dimensional excitation and emission matrix fluorescence (3DEEM) for quick and pseudo-quantitative determination of protein- and humic-like substances in full-scale membrane bioreactor (MBR). Water Res 118, 82–92. https://doi.org/10.1016/j.watres.2017.04.009

Jeison, D., van Lier, J.B., 2006. Cake layer formation in anaerobic submerged membrane bioreactors (AnSMBR) for wastewater treatment. Journal of Membrane Science 284, 227–236. https://doi.org/10.1016/j.memsci.2006.07.035

Ji, J., Chen, Y., Hu, Y., Ohtsu, A., Ni, J., Li, Y., Sakuma, S., Hojo, T., Chen, R., Li, Y.-Y., 2021a. One-year operation of a 20-L submerged anaerobic membrane bioreactor for real domestic wastewater treatment at room temperature: Pursuing the optimal HRT and sustainable flux. Science of The Total Environment 775, 145799. https://doi.org/10.1016/j.scitotenv.2021.145799

Ji, J., Du, R., Ni, J., Chen, Y., Hu, Y., Qin, Y., Hojo, T., Li, Y.-Y., 2022. Submerged anaerobic membrane bioreactor applied for mainstream municipal wastewater treatment at a low

652   temperature: Sludge yield, energy balance and membrane filtration behaviors. Journal
653   of Cleaner Production 355, 131831. https://doi.org/10.1016/j.jclepro.2022.131831
654 Ji, J., Ni, J., Ohtsu, A., Isozumi, N., Hu, Y., Du, R., Chen, Y., Qin, Y., Kubota, K., Li, Y.-Y.,
655   2021b. Important effects of temperature on treating real municipal wastewater by a
656   submerged anaerobic membrane bioreactor: Removal efficiency, biogas, and microbial
657   community. Bioresour Technol 336, 125306.
658   https://doi.org/10.1016/j.biortech.2021.125306
659 Kaya, Y., Bacaksiz, A.M., Bayrak, H., Gönder, Z.B., Vergili, I., Hasar, H., Yilmaz, G., 2017.
660   Treatment of chemical synthesis-based pharmaceutical wastewater in an ozonation-
661   anaerobic membrane bioreactor (AnMBR) system. Chemical Engineering Journal 322,
662   293–301. https://doi.org/10.1016/j.cej.2017.03.154
663 Kaya, Y., Bacaksiz, A.M., Bayrak, H., Vergili, I., Gönder, Z.B., Hasar, H., Yilmaz, G., 2019.
664   Investigation of membrane fouling in an anaerobic membrane bioreactor (AnMBR)
665   treating pharmaceutical wastewater. Journal of Water Process Engineering 31, 100822.
666   https://doi.org/10.1016/j.jwpe.2019.100822
667 Kong, Z., Li, L., Wu, J., Wang, T., Rong, C., Luo, Z., Pan, Y., Li, D., Li, Y., Huang, Y., Li, Y.-
668   Y., 2021a. Evaluation of bio-energy recovery from the anaerobic treatment of municipal
669   wastewater by a pilot-scale submerged anaerobic membrane bioreactor (AnMBR) at
670   ambient temperature. Bioresource Technology 339, 125551.
671   https://doi.org/10.1016/j.biortech.2021.125551
672 Kong, Z., Wu, J., Rong, C., Wang, T., Li, L., Luo, Z., Ji, J., Hanaoka, T., Sakemi, S., Ito, M.,
673   Kobayashi, S., Kobayashi, M., Qin, Y., Li, Y.-Y., 2021b. Large pilot-scale submerged
674   anaerobic membrane bioreactor for the treatment of municipal wastewater and biogas
675   production at 25 °C. Bioresour Technol 319, 124123.
676   https://doi.org/10.1016/j.biortech.2020.124123
677 Layer, M., Adler, A., Reynaert, E., Hernandez, A., Pagni, M., Morgenroth, E., Holliger, C.,
678   Derlon, N., 2019. Organic substrate diffusibility governs microbial community
679   composition, nutrient removal performance and kinetics of granulation of aerobic
680   granular sludge. Water Research X 4, 100033.
681   https://doi.org/10.1016/j.wroa.2019.100033
682 Lei, Z., Yang, S., Li, Y., Wen, W., Wang, X.C., Chen, R., 2018. Application of anaerobic
683   membrane bioreactors to municipal wastewater treatment at ambient temperature: A
684   review of achievements, challenges, and perspectives. Bioresource Technology 267,
685   756–768. https://doi.org/10.1016/j.biortech.2018.07.050
686 Li, X.Y., Yang, S.F., 2007. Influence of loosely bound extracellular polymeric substances
687   (EPS) on the flocculation, sedimentation and dewaterability of activated sludge. Water
688   Research 41, 1022–1030. https://doi.org/10.1016/j.watres.2006.06.037
689 Lin, H., Peng, W., Zhang, M., Chen, J., Hong, H., Zhang, Y., 2013. A review on anaerobic
690   membrane bioreactors: Applications, membrane fouling and future perspectives.
691   Desalination 314, 169–188. https://doi.org/10.1016/j.desal.2013.01.019
692 Lowry, OliverH., Rosebrough, NiraJ., Farr, A.L., Randall, RoseJ., 1951. Protein measurement
693   with the Folin phenol reagent. Journal of Biological Chemistry 193, 265–275.
694   https://doi.org/10.1016/S0021-9258(19)52451-6
695 Maaz, M., Yasin, M., Aslam, M., Kumar, G., Atabani, A.E., Idrees, M., Anjum, F., Jamil, F.,
696   Ahmad, R., Khan, A.L., Lesage, G., Heran, M., Kim, J., 2019. Anaerobic membrane
697   bioreactors for wastewater treatment: Novel configurations, fouling control and energy
698   considerations. Bioresource Technology 283, 358–372.
699   https://doi.org/10.1016/j.biortech.2019.03.061
700 Martinez-Sosa, D., Helmreich, B., Netter, T., Paris, S., Bischof, F., Horn, H., 2011. Anaerobic
701   submerged membrane bioreactor (AnSMBR) for municipal wastewater treatment under

mesophilic and psychrophilic temperature conditions. Bioresource Technology 102, 10377–10385. https://doi.org/10.1016/j.biortech.2011.09.012

Martin-Garcia, I., Mokosch, M., Soares, A., Pidou, M., Jefferson, B., 2013. Impact on reactor configuration on the performance of anaerobic MBRs: Treatment of settled sewage in temperate climates. Water Research 47, 4853–4860. https://doi.org/10.1016/j.watres.2013.05.008

Nie, Y., Kato, H., Sugo, T., Hojo, T., Tian, X., Li, Y.-Y., 2017. Effect of anionic surfactant inhibition on sewage treatment by a submerged anaerobic membrane bioreactor: Efficiency, sludge activity and methane recovery. Chemical Engineering Journal 315, 83–91. https://doi.org/10.1016/j.cej.2017.01.022

Plevri, A., Mamais, D., Noutsopoulos, C., 2021. Anaerobic MBR technology for treating municipal wastewater at ambient temperatures. Chemosphere 275, 129961. https://doi.org/10.1016/j.chemosphere.2021.129961

Quek, P.J., Yeap, T.S., Ng, H.Y., 2017. Applicability of upflow anaerobic sludge blanket and dynamic membrane-coupled process for the treatment of municipal wastewater. Appl Microbiol Biotechnol 101, 6531–6540. https://doi.org/10.1007/s00253-017-8358-6

Robles, Á., Durán, F., Giménez, J.B., Jiménez, E., Ribes, J., Serralta, J., Seco, A., Ferrer, J., Rogalla, F., 2020. Anaerobic membrane bioreactors (AnMBR) treating urban wastewater in mild climates. Bioresource Technology 314, 123763. https://doi.org/10.1016/j.biortech.2020.123763

Robles, A., Ruano, M.V., Ribes, J., Seco, A., Ferrer, J., 2014. Model-based automatic tuning of a filtration control system for submerged anaerobic membrane bioreactors (AnMBR). Journal of Membrane Science 465, 14–26. https://doi.org/10.1016/j.memsci.2014.04.012

Rong, C., Luo, Z., Wang, T., Guo, Y., Kong, Z., Wu, J., Ji, J., Qin, Y., Hanaoka, T., Sakemi, S., Ito, M., Kobayashi, S., Kobayashi, M., Li, Y.-Y., 2021. Chemical oxygen demand and nitrogen transformation in a large pilot-scale plant with a combined submerged anaerobic membrane bioreactor and one-stage partial nitritation-anammox for treating mainstream wastewater at 25 °C. Bioresource Technology 341, 125840. https://doi.org/10.1016/j.biortech.2021.125840

Ruigómez, I., Vera, L., González, E., González, G., Rodríguez-Sevilla, J., 2016a. A novel rotating HF membrane to control fouling on anaerobic membrane bioreactors treating wastewater. Journal of Membrane Science 501, 45–52. https://doi.org/10.1016/j.memsci.2015.12.011

Ruigómez, I., Vera, L., González, E., Rodríguez-Sevilla, J., 2016b. Pilot plant study of a new rotating hollow fibre membrane module for improved performance of an anaerobic submerged MBR. Journal of Membrane Science 514, 105–113. https://doi.org/10.1016/j.memsci.2016.04.061

Sanchez, L., Carrier, M., Cartier, J., Charmette, C., Heran, M., Steyer, J.-P., Lesage, G., 2022. Enhanced organic degradation and biogas production of domestic wastewater at psychrophilic temperature through submerged granular anaerobic membrane bioreactor for energy-positive treatment. Bioresource Technology 353, 127145. https://doi.org/10.1016/j.biortech.2022.127145

Shin, C., Tilmans, S.H., Chen, F., McCarty, P.L., Criddle, C.S., 2021. Temperate climate energy-positive anaerobic secondary treatment of domestic wastewater at pilot-scale. Water Research 204, 117598. https://doi.org/10.1016/j.watres.2021.117598

Smith, A.L., Skerlos, S.J., Raskin, L., 2013. Psychrophilic anaerobic membrane bioreactor treatment of domestic wastewater. Water Research 47, 1655–1665. https://doi.org/10.1016/j.watres.2012.12.028

Smith, A.L., Stadler, L.B., Cao, L., Love, N.G., Raskin, L., Skerlos, S.J., 2014. Navigating Wastewater Energy Recovery Strategies: A Life Cycle Comparison of Anaerobic Membrane Bioreactor and Conventional Treatment Systems with Anaerobic Digestion. Environ. Sci. Technol. 48, 5972–5981. https://doi.org/10.1021/es5006169

Smith, A.L., Stadler, L.B., Love, N.G., Skerlos, S.J., Raskin, L., 2012. Perspectives on anaerobic membrane bioreactor treatment of domestic wastewater: A critical review. Bioresource Technology 122, 149–159. https://doi.org/10.1016/j.biortech.2012.04.055

Stuckey, D.C., 2012. Recent developments in anaerobic membrane reactors. Bioresource Technology, Membrane Bioreactors (MBRs): State-of-Art and Future 122, 137–148. https://doi.org/10.1016/j.biortech.2012.05.138

van Lier, J.B., Mahmoud, N., Zeeman, G., 2008. Anaerobic Wastewater Treatment, in: Biological Wastewater Treatment: Principles, Medelling and Design. IWA Publishing.

Vinardell, S., Astals, S., Peces, M., Cardete, M.A., Fernández, I., Mata-Alvarez, J., Dosta, J., 2020. Advances in anaerobic membrane bioreactor technology for municipal wastewater treatment: A 2020 updated review. Renewable and Sustainable Energy Reviews 130, 109936. https://doi.org/10.1016/j.rser.2020.109936

Vinardell, S., Sanchez, L., Astals, S., Mata-Alvarez, J., Dosta, J., Heran, M., Lesage, G., 2022. Impact of permeate flux and gas sparging rate on membrane performance and process economics of granular anaerobic membrane bioreactors. Science of The Total Environment 825, 153907. https://doi.org/10.1016/j.scitotenv.2022.153907

Wang, K.M., Cingolani, D., Eusebi, A.L., Soares, A., Jefferson, B., McAdam, E.J., 2018. Identification of gas sparging regimes for granular anaerobic membrane bioreactor to enable energy neutral municipal wastewater treatment. Journal of Membrane Science 555, 125–133. https://doi.org/10.1016/j.memsci.2018.03.032

Watanabe, R., Nie, Y., Wakahara, S., Komori, D., Li, Y.-Y., 2017. Investigation on the response of anaerobic membrane bioreactor to temperature decrease from 25°C to 10°C in sewage treatment. Bioresource Technology 243, 747–754. https://doi.org/10.1016/j.biortech.2017.07.001

Yang, G., Zhang, P., Zhang, G., Wang, Y., Yang, A., 2015. Degradation properties of protein and carbohydrate during sludge anaerobic digestion. Bioresource Technology 192, 126–130. https://doi.org/10.1016/j.biortech.2015.05.076

Yang, Y., Zang, Y., Hu, Y., Wang, X.C., Ngo, H.H., 2020. Upflow anaerobic dynamic membrane bioreactor (AnDMBR) for wastewater treatment at room temperature and short HRTs: Process characteristics and practical applicability. Chemical Engineering Journal 383, 123186. https://doi.org/10.1016/j.cej.2019.123186

Yao, W., Hou, L., Wang, F., Wang, Z., Zhang, H., 2022. Dual-objective for the mechanism of membrane fouling in the early stage of filtration and determination of cleaning frequency: A novel combined model. Journal of Membrane Science 647, 120315. https://doi.org/10.1016/j.memsci.2022.120315

Yao, Y., Zhou, Z., Stuckey, D.C., Meng, F., 2020. Micro-particles—A Neglected but Critical Cause of Different Membrane Fouling between Aerobic and Anaerobic Membrane Bioreactors. ACS Sustainable Chem. Eng. 8, 16680–16690. https://doi.org/10.1021/acssuschemeng.0c06502

Yeo, H., An, J., Reid, R., Rittmann, B.E., Lee, H.-S., 2015. Contribution of Liquid/Gas Mass-Transfer Limitations to Dissolved Methane Oversaturation in Anaerobic Treatment of Dilute Wastewater. Environ. Sci. Technol. 49, 10366–10372. https://doi.org/10.1021/acs.est.5b02560

Zhou, Z., Tan, Y., Xiao, Y., Stuckey, D.C., 2016. Characterization and Significance of Sub-Visible Particles and Colloids in a Submerged Anaerobic Membrane Bioreactor

800   (SAnMBR).   Environ.   Sci.   Technol.   50,   12750–12758.
801   https://doi.org/10.1021/acs.est.6b03581
802